

Josephson junctions with tunable current-phase relation

A. Lipman,¹ R. G. Mints,¹ R. Kleiner,² D. Koelle,² and E. Goldobin^{2,*}

¹The Raymond and Beverly Sackler School of Physics and Astronomy, Tel Aviv University, Tel Aviv 69978, Israel

²Physikalisches Institut und Center for Collective Quantum Phenomena in LISA⁺, Universität Tübingen,
Auf der Morgenstelle 14, D-72076 Tübingen, Germany

(Received 29 September 2014; revised manuscript received 22 October 2014; published 7 November 2014)

We consider $0-\pi$ Josephson junctions consisting of 0 and π regions of lengths L_0 and L_π with critical current densities j_{c0} and $j_{c\pi}$, respectively. The dependence of the Josephson current on the phase-shift averaged along the junction is derived. We show that these systems exhibit the main features of φ Josephson junctions—the ground state is doubly degenerate and the current-phase relation can be tuned *in situ* by applying magnetic field. In the limit of short and long 0 and π regions, the current phase relation is derived analytically. In the case of intermediate lengths of 0 and π regions, the current-phase relation is calculated numerically.

DOI: [10.1103/PhysRevB.90.184502](https://doi.org/10.1103/PhysRevB.90.184502)

PACS number(s): 74.50.+r, 85.25.Cp

I. INTRODUCTION

Usually, Josephson junctions (JJs) have a phase drop $\phi = 0$ in the ground state, *i.e.* when no current is applied. Recently, Josephson junctions with a nonzero ground-state phase $\phi \neq 0$ attracted strong attention [1–7]. Most of these JJs are π Josephson junctions. Several types of JJs with the ground-state phase $\phi = \varphi$ were suggested recently [8–11] and implemented experimentally [12,13]. In general, a φ Josephson junction can be defined as a junction having a degenerate Josephson phase $\phi = \pm\varphi$ in the ground state. In terms of Josephson energy (potential), this corresponds to a 2π periodic double well, where the phase has two degenerate minima $\phi = \pm\varphi + 2\pi n$, where n is an integer. The evidence of φ JJs in high- T_c grain boundary JJs was presented [14], where noninteger *splintered* Josephson vortices were observed in agreement with theory [15,16]. φ JJs have very interesting properties that are important for applications [13] as well as for fundamental physics [17,18].

Initially, we suggested [11] to implement a φ JJ with a magnetic-field tunable current-phase relation (CPR) based on a $0-\pi$ JJ with its 0 and π segments of different length $L_0 \neq L_\pi$ (see Fig. 1 for the geometry of the problem). This study was motivated by technology of JJs fabricated between *d*-wave and *s*-wave superconductors [19–21]. However, in the experiment reported in Ref. [12] we were able to demonstrate φ JJs based on superconductor-insulator-ferromagnet-superconductor (SIFS) $0-\pi$ JJs [22–24], where the lengths of the 0 and π segments were nominally equal, but critical current densities j_{c0} and $j_{c\pi}$ in the 0 and π parts were different. Therefore, the theory [11] should be generalized to the more general case $j_{c0} \neq j_{c\pi}$.

Furthermore, the theoretical approach from Ref. [11] is only applicable in a narrow region of the parameter space. This makes it almost impossible to realize experimentally a $0-\pi$ JJ that is located in this region. This can be corrected by deriving the CPR in the two limiting cases of short and long φ JJs analytically and studying the CPR in the region of parameters between the both limiting cases numerically. The main target of this paper is to find the CPR of a φ JJ in the whole parameter space, for any j_{c0} , $j_{c\pi}$, L_0 , L_π .

The paper is organized as follows. In Sec. II we introduce the model that we use for the general case $j_{c0} \neq j_{c\pi}$ and $L_0 \neq L_\pi$. In Sec. III we present the analytically calculated CPR obtained in the limits of short and long JJs as well as the numerically calculated CPR in the case of intermediate lengths. In Sec. IV we discuss the phase diagrams. A summary, Sec. V, concludes the paper.

II. BASIC EQUATIONS

The static spatial distribution of the phase difference $\phi(x)$ along the JJ (see Fig. 1 for definitions of j_{c0} , $j_{c\pi}$, L_0 , L_π and the geometry) is described by the sine-Gordon equation

$$\frac{\Phi_0}{2\pi\mu_0d_J} \phi'' - j_c(x) \sin \phi = -j, \quad (1)$$

where Φ_0 is the magnetic flux quantum, μ_0d_J is the specific inductance (per square) of the superconducting banks forming the JJ, $j_c(x)$ is the Josephson critical current density, j is the bias current density, the prime denotes the derivative with respect to the coordinate x . We assume that the critical current density $j_c(x)$ is a stepwise function,

$$j_c(x) = \begin{cases} j_{c0}, & 0 \leq x \leq L_0, \\ -j_{c\pi}, & -L_\pi \leq x < 0, \end{cases} \quad (2)$$

where both critical current densities j_{c0} and $j_{c\pi}$ are positive constants. It is convenient to write $j_c(x)$ in the form [15]

$$j_c(x) = \langle j_c(x) \rangle [1 + g(x)], \quad (3)$$

where the average $\langle j_c(x) \rangle$ is defined by

$$\langle j_c(x) \rangle = \frac{1}{L} \int_{-L_\pi}^{L_0} j_c(x) dx = \frac{1}{L} (j_{c0}L_0 - j_{c\pi}L_\pi), \quad (4)$$

$L = L_0 + L_\pi$ is the total length of the junction, and $\langle g(x) \rangle = 0$. The function $g(x)$ is defined by Eq. (3) and takes the form

$$g(x) = \frac{j_c(x)}{\langle j_c(x) \rangle} - 1, \quad (5)$$

with the stepwise dependence of the function $g(x)$ on x ,

$$g(x) = \begin{cases} g_0, & 0 < x < L_0, \\ g_\pi, & -L_\pi < x < 0, \end{cases} \quad (6)$$

*gold@uni-tuebingen.de

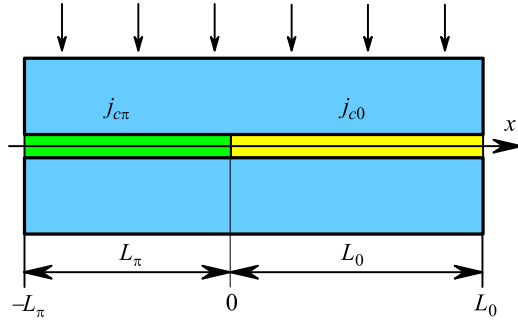


FIG. 1. (Color online) Sketch of the geometry of the φ JJ. The region $0 < x < L_0$ is a 0-JJ and the region $-L_\pi < x < 0$ is a π -JJ.

where

$$g_0 = \frac{(j_{c0} + j_{c\pi})L_\pi}{j_{c0}L_0 - j_{c\pi}L_\pi}, \quad g_\pi = -\frac{(j_{c0} + j_{c\pi})L_0}{j_{c0}L_0 - j_{c\pi}L_\pi} \quad (7)$$

are constants defined by the properties and structure of the JJ.

Next, we normalize the coordinate x by a certain length (making it dimensionless) to simplify the theoretical approach to the problem. There are two primary options defined by the typical lengths, which are convenient for the coordinate normalization—*global* [15] and *local* [25].

A. Global normalization

In this case we normalize the coordinate x by $\lambda_{Jg} \propto 1/\sqrt{\langle |j_c| \rangle}$, where the averaging is over the whole junction. Here, the *global* Josephson penetration depth λ_{Jg} is defined by the value of the average critical current density $\langle j_c \rangle$ and is given by [15]

$$\lambda_{Jg} = \sqrt{\frac{\Phi_0}{2\pi\mu_0 d_J \langle |j_c| \rangle}}. \quad (8)$$

The dimensionless coordinate x lies then within the interval

$$-l_\pi \equiv -\frac{L_\pi}{\lambda_{Jg}} \leq x \leq \frac{L_0}{\lambda_{Jg}} \equiv l_0. \quad (9)$$

Using the dimensionless coordinate x we write Eq. (1) in the form

$$\phi'' - \text{sgn}(\langle j_c \rangle)[1 + g(x)] \sin \phi = -\gamma, \quad (10)$$

where $\gamma = j/\langle j_c \rangle$ is the normalized bias current density. By introducing the new phase,

$$\hat{\phi} = \begin{cases} \phi & \langle j_c \rangle > 0 \\ \pi - \phi & \langle j_c \rangle < 0 \end{cases}, \quad (11)$$

we can rewrite Eq. (10) as

$$\hat{\phi}'' - [1 + g(x)] \sin \hat{\phi} = -\gamma. \quad (12)$$

As shown below, the global normalization is convenient for the theoretical analysis of the problem in the short junction limit.

B. Local normalization

In this case we normalize the x coordinate differently in the 0 region and in the π region by using two different “stretching”

factors. In the interval $-L_\pi \leq x \leq 0$ we normalize x as $x/\lambda_{J\pi}$ and in the region $0 \leq x \leq L_0$ we normalize x as x/λ_{J0} , where

$$\lambda_{J0} = \sqrt{\frac{\Phi_0}{2\pi\mu_0 d_J j_{c0}}}, \quad \lambda_{J\pi} = \sqrt{\frac{\Phi_0}{2\pi\mu_0 d_J j_{c\pi}}} \quad (13)$$

are the local Josephson penetration depths [25]. It is seen from Eq. (13) that the dimensionless coordinate x lies now within the interval $-\ell_\pi < x < \ell_0$, where

$$\ell_\pi = \frac{L_\pi}{\lambda_{J\pi}}, \quad \ell_0 = \frac{L_0}{\lambda_{J0}}. \quad (14)$$

It is shown below that the local normalization is convenient for comparison of the numerically calculated and measured data, and it must be used for phase diagrams in the L_0, L_π plane.

III. CURRENT PHASE RELATION

A. Numerical simulations

We begin the study of the CPRs from numerical simulations of Eq. (10). The procedure used for these calculations is as follows. First, we chose a certain set of parameters $L_0, L_\pi, j_{c0}/\langle j_c(x) \rangle, j_{c\pi}/\langle j_c(x) \rangle$ and a bias current γ . Second, we solve Eq. (10) for each of these sets. As a result we obtain one or more solutions for the function $\phi(x)$. Next, for each of these solutions we calculate the spatial average $\psi = \langle \phi(x) \rangle$ and plot these values of ψ on a $\psi(\gamma)$ plot. If we repeat this procedure for different values of γ we obtain $\gamma(\psi)$, the *effective* current-phase relation.

B. Short junctions

In the case of short JJ the current-phase relation can be obtained analytically. It is convenient to derive it by using the global normalization for the following calculations. First, we write the solution of Eq. (12) in the form

$$\hat{\phi}(x) = \hat{\psi} + \xi(x) \sin \hat{\psi}, \quad (15)$$

where $\hat{\psi}$ is the spatial average of $\hat{\phi}(x)$. $\hat{\psi}$ is related to the true average phase ψ via an equation similar to Eq. (11). The term $\xi(x) \sin \hat{\psi}$ describes the deviation of the phase from its average value, $\langle \xi(x) \rangle = 0$. Next, we assume that this deviation is small, $|\xi(x) \sin \hat{\psi}| \ll 1$. Then we plug the relation given by Eq. (15) into Eq. (10), expand it in series in $\xi(x) \sin \hat{\psi}$, and keep the terms of zero and first order. As a result we find

$$\xi'' \sin \hat{\psi} - [1 + g(x)][1 + \xi(x) \cos \hat{\psi}] \sin \hat{\psi} = -\gamma. \quad (16)$$

The zero- and second-order terms in ξ in Eq. (16) are given by the following two equations:

$$\gamma = \sin \hat{\psi} + \langle \xi(x)g(x) \rangle \cos \hat{\psi} \sin \hat{\psi}, \quad (17)$$

$$\xi'' - g(x) = [\xi + \xi(x)g(x) - \langle \xi(x)g(x) \rangle] \cos \hat{\psi}. \quad (18)$$

Numerical calculations show that the terms $\propto \cos \hat{\psi}$ have an extremely weak effect on the solutions of Eq. (18) when facet lengths are small $l_0, l_\pi \ll 1$. We neglect these terms and obtain for $\xi(x)$

$$\xi'' - g(x) = 0. \quad (19)$$

The solutions of Eq. (19) are continuous at $x = 0$ and match the boundary conditions at $x = -l_\pi$ and $x = l_0$:

$$\xi_0(0) = \xi_0(0), \quad \xi'_\pi(0) = \xi'_0(0), \quad (20)$$

$$\xi'_\pi(-l_\pi) \sin \hat{\psi} = h, \quad \xi'_0(l_0) \sin \hat{\psi} = h. \quad (21)$$

The magnetic field H applied normal to the plane of Fig. 1 is normalized by $H_{c1}/2$,

$$h = \frac{2H}{H_{c1}}, \quad H_{c1} = \frac{\Phi_0}{\pi \Lambda \lambda_{Jg}}, \quad (22)$$

where Λ is the effective magnetic thickness of the JJ.

We integrate Eq. (19) by using boundary condition Eqs. (20) and (21) and obtain

$$\xi_0(x) = g_0 \left(\frac{x^2}{2} - l_0 x \right) + \frac{hx}{\sin \hat{\psi}} + C, \quad \text{for} \quad 0 < x < l_0, \quad (23)$$

$$\xi_\pi(x) = g_\pi \left(\frac{x^2}{2} + l_\pi x \right) + \frac{hx}{\sin \hat{\psi}} + C, \quad \text{for} \quad -l_\pi < x < 0. \quad (24)$$

The integration constant C can be obtained by using the condition $\langle \xi(x) \rangle = 0$, which yields

$$C = \frac{l_0 - l_\pi}{2} \left(\frac{g_0 l_0 + g_\pi l_\pi}{3} - \frac{h}{\sin \hat{\psi}} \right). \quad (25)$$

We use Eqs. (6), (23), and (24) to obtain the average $\langle \xi(x)g(x) \rangle$ in the form

$$\langle \xi(x)g(x) \rangle = \Gamma_0 + \Gamma_h \frac{h}{\sin \hat{\psi}}, \quad (26)$$

where the coefficients Γ_0 and Γ_h are given by

$$\Gamma_0 = -\frac{l_0^2 l_\pi^2}{3} \frac{(j_{c0} + j_{c\pi})^2}{(j_{c0} l_0 - j_{c\pi} l_\pi)^2}, \quad (27)$$

$$\Gamma_h = \frac{l_0 l_\pi}{2} \frac{j_{c0} + j_{c\pi}}{j_{c0} l_0 - j_{c\pi} l_\pi}. \quad (28)$$

Using Eqs. (17) and (26) we find the current-phase relation in the form

$$j = \langle j_c \rangle (\sin \psi \pm \Gamma_0 \sin \psi \cos \psi \pm h \Gamma_h \cos \psi), \quad (29)$$

where \pm stands for $\langle j_c \rangle > 0$ and $\langle j_c \rangle < 0$, respectively. It is worth noting that there is a simple relation between the coefficients Γ_0 and Γ_h . Indeed, it follows from Eqs. (27) and (28) that

$$\Gamma_0 = -\frac{4}{3} \Gamma_h^2. \quad (30)$$

In particular, in the case of equal lengths of 0 and π regions ($l_0 = l_\pi$) we find

$$\Gamma_0 = -\frac{l^2}{12} \left(\frac{j_{c0} + j_{c\pi}}{j_{c0} - j_{c\pi}} \right)^2, \quad (31)$$

$$\Gamma_h = \frac{l}{4} \frac{j_{c0} + j_{c\pi}}{j_{c0} - j_{c\pi}}, \quad (32)$$

where $l = 2l_0 = 2l_\pi$.

TABLE I. Parameters of the JJs used as illustrative examples.

JJ name	j_{c0}	$j_{c\pi}$	l_0	l_π	ℓ_0	ℓ_π
a	1.0	1.0	1.155	0.577	2.00	1.00
b	1.0	1.0	1.342	1.894	3.00	2.00
c	1.0	1.0	2.500	1.500	5.00	3.00
d	1.0	0.5	1.155	1.155	2.309	1.633
e	1.0	0.5	2.309	2.309	4.619	3.266
f	1.0	0.5	3.819	2.291	5.774	2.449

C. Long junctions

In the case of *long* JJ facets, for $1 \ll \ell_0, \ell_\pi$ we neglect the spatial variation of the phase in the vicinity of the $0-\pi$ interface ($|x| \ll \lambda_{J0}, \lambda_{J\pi}$). In this approximation the values of the phases are

$$\phi(x) \approx \begin{cases} \pm\pi - \arcsin(j/j_{c\pi}), & x < 0, \\ \arcsin(j/j_{c0}), & x > 0. \end{cases} \quad (33)$$

It follows from Eq. (33) that in the case of a long JJ the average phase ψ is given by

$$\psi = \frac{L_0}{L} \arcsin \frac{j}{j_{c0}} + \frac{L_\pi}{L} \left(\pm\pi - \arcsin \frac{j}{j_{c\pi}} \right). \quad (34)$$

The above equation defines the CPR $j(\psi)$ in a long JJ. The maximum supercurrent for this system was calculated in Ref. [26].

In the next approximation $1/\ell_0 \ll 1$ and $1/\ell_\pi \ll 1$ we take into account the spatial dependence of the phase $\phi(x)$ in the vicinity of the $0-\pi$ interface. As a result it can be shown that the function $\phi(x)$ describes a semifluxon pinned at the $0-\pi$ interface (see Appendices A and C for details).

D. Discussion

In the following we show current-phase relations obtained by each of the above techniques for different facet lengths and for different relations between the critical current densities of the 0 and π regions. The parameters of the JJs used as examples are summarized in Table I.

Several examples of the CPRs are shown in Fig. 2. One can see that for shorter $0-\pi$ JJs, the CPR has two stable static solutions (ground states) with the phase $\psi = \pm\varphi$. However, as the length of the JJ increases, one can observe regions of negative slope; see Fig. 2(c). This implies a bistability and abrupt switching of the system between two CPR branches. Also, at even larger lengths one can observe multiple branches corresponding to the appearance of additional solutions; see Figs. 2(c), 2(e), and 2(f). In terms of a reliable application of φ JJs such regimes with multiple solutions should be avoided.

In Fig. 2, apart from numerically calculated CPRs we show CPRs obtained in the limits of short and long JJs analytically for different facets lengths and for different relations between the critical currents densities in the 0 and π regions. One can see that indeed for short 0 and π regions the short-limit formula, Eq. (29), reproduces the CPR quite well. For longer JJs, Eq. (29) predicts a much larger amplitude of the supercurrent (critical current) than what follows from direct simulations. The long-limit formula, Eq. (34), obviously works

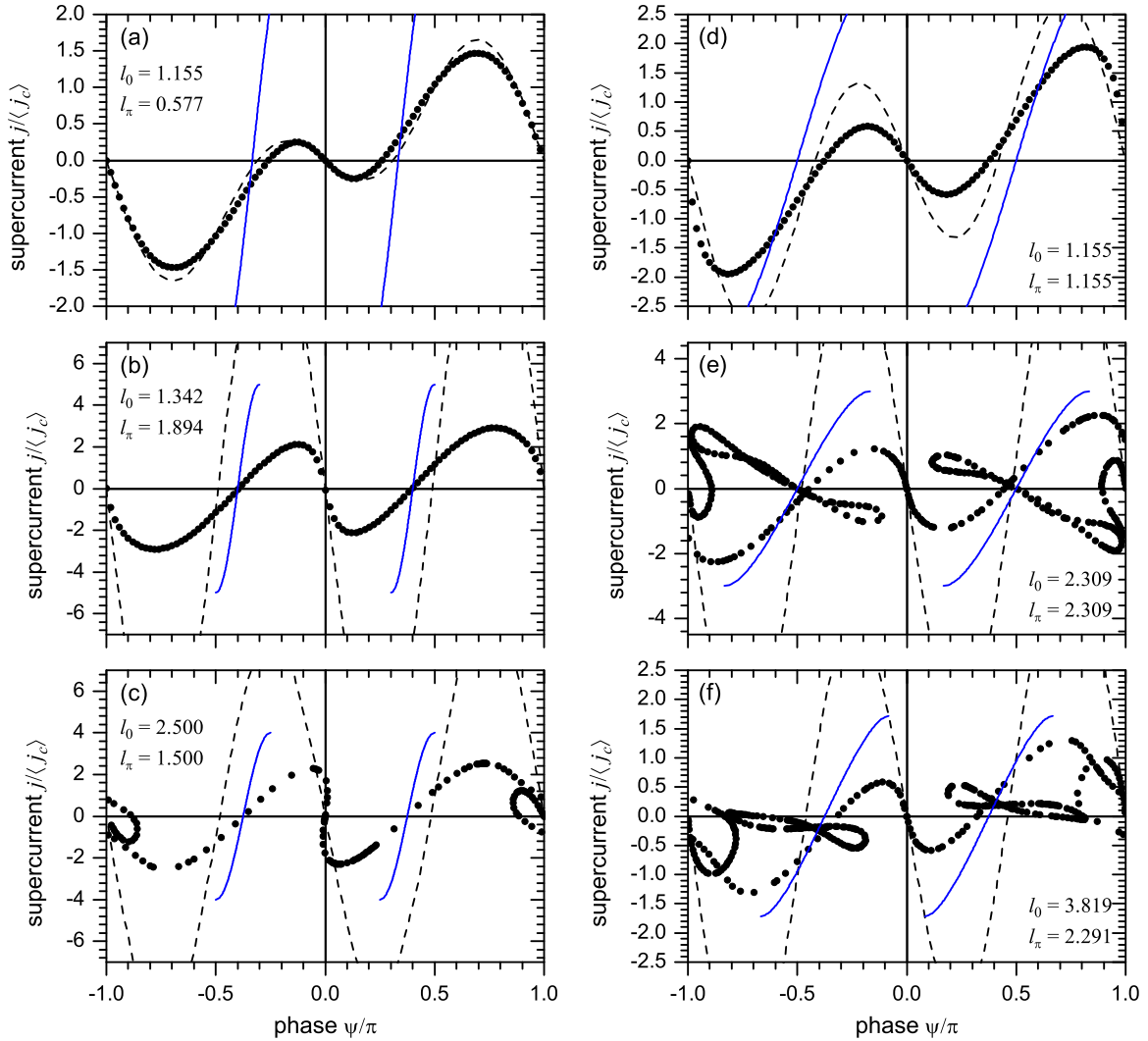


FIG. 2. (Color online) CPR in a $0\text{-}\pi$ JJ with $j_{c0} = j_{c\pi}$ (a)–(c) and $j_{c0} = 2j_{c\pi}$ (d)–(f) for different normalized lengths l_0 and l_π . The black dots show the numerically calculated CPR. The CPR given by the short limit formula, Eq. (29), is shown by the dashed line. The CPR (stable branch) given by the long limit formula, Eq. (34), is shown by the solid (blue) lines.

better for larger lengths of the 0 and π parts. However, at best, it only reproduces correctly the value of the ground-state phase φ but not the slope of the CPR. This is expected as the formula does not take into account the bending of the phase near $x = 0$. Thus, it may work better for $L \sim 100$, which is not relevant for current experiments. Moreover, for $L \sim 100$ the system under consideration will have so many competing solutions (CPR branches) that its real application will be problematic.

IV. PHASE DIAGRAMS

The phase diagrams in Figs. 3 (symmetric junction, $j_{c0} = j_{c\pi}$) and 4 (asymmetric junction, as an example we take $j_{c0} = 2j_{c\pi}$) show the domains of existence of φ states in the l_0, l_π plane and contours of constant ground-state phase φ ($\varphi \equiv \psi @ j = 0$ and $dj/d\psi|_{j=0} > 0$). We also demonstrate comparison of numerically calculated constant phase contours with analytically calculated ones for the limiting cases of short and long junctions, for $l_0 \ll 1, l_\pi \ll 1$, and $l_0 \gg 1, l_\pi \gg 1$. Moreover, a comparison between the phase diagrams of Figs. 3

and 4 shows how junction asymmetry affects the spreading and bending of the φ contours.

A. Theoretical calculation for short JJ

We begin with treating the phase diagrams for the limiting case of short junctions. Using Eqs. (27) and (29) with $h = 0$ and $j = 0$ (ground state) we find that the phase in the ground-state φ obeys

$$1 + \Gamma_0 \cos \varphi = 0, \quad (35)$$

and the lengths $l_\pi(l_0)$ and $l_0(l_\pi)$ have the form (rewritten in the local normalization)

$$l_\pi(l_0) = \frac{l_0}{2} \sqrt{3j_{c0}j_{c\pi}} \frac{\sqrt{3}j_\Sigma + j_\Delta \sqrt{3 + 4l_0^2 \cos \varphi}}{\ell_0^2 j_\Delta^2 \cos \varphi - 3j_{c0}j_{c\pi}}, \quad (36)$$

$$l_0(l_\pi) = \frac{l_\pi}{2} \sqrt{3j_{c0}j_{c\pi}} \frac{\sqrt{3}j_\Sigma - j_\Delta \sqrt{3 - 4l_\pi^2 \cos \varphi}}{\ell_\pi^2 j_\Delta^2 \cos \varphi + 3j_{c0}j_{c\pi}}, \quad (37)$$

where $j_\Sigma = j_{c0} + j_{c\pi}$ and $j_\Delta = |j_{c0} - j_{c\pi}|$.

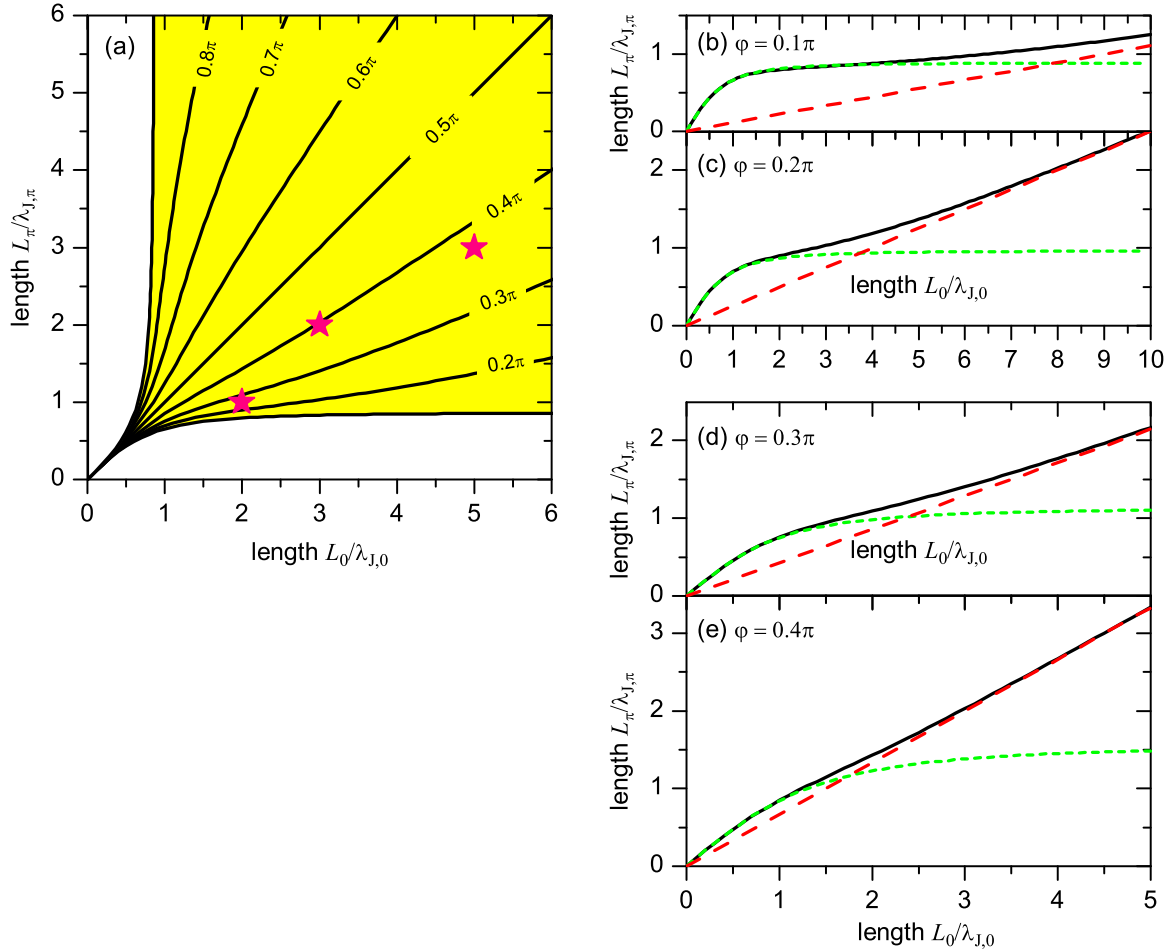


FIG. 3. (Color online) Phase diagrams calculated for the case $j_{c0} = j_{c\pi}$. (a) The contour lines of constant ground-state phase φ calculated numerically (solid lines). The numbers interrupting the lines indicate the values of φ . The filled region is the domain of interest where the phase smoothly changes between 0 and π . The stars show the parameters of the samples a, b, and c from Table I. (b)–(e) Comparison between the numerically calculated solid lines of constant phase with those calculated analytically in the short limit (green short dashed lines) and long limit (red dashed lines).

It is worth mentioning that Eqs. (36) and (37) are valid for any value of φ within the interval $0 \leq \varphi \leq \pi$. However, for $\varphi \leq \pi/2$ it is more convenient to use Eq. (36), as Eq. (37) has a singularity at $\ell_\pi = \sqrt{-3j_{c0}j_{c\pi}/(j_\Delta^2 \cos \varphi)}$. In the case of $\varphi > \pi/2$ then we use Eq. (37) for any ℓ_π , while Eq. (36) diverges at $\ell_0 = \sqrt{2j_{c0}j_{c\pi}/(j_\Delta^2 \cos \varphi)}$.

Finally, we note that in the global normalization the formulas given by Eqs. (36) and (37) read

$$l_\pi(l_0) = j_{c0}l_0 \frac{3j_{c\pi} - l_0j_\Delta \operatorname{sgn}(\cos \varphi)\sqrt{3|\cos \varphi|}}{l_0^2j_\Delta^2|\cos \varphi| - 3j_{c0}^2}, \quad (38)$$

$$l_0(l_\pi) = j_{c\pi}l_\pi \frac{3j_{c0} + l_\pij_\Delta \operatorname{sgn}(\cos \varphi)\sqrt{3|\cos \varphi|}}{l_\pi^2j_\Delta^2\cos \varphi - 3j_{c0}^2}. \quad (39)$$

B. Analytical calculation for a long JJ

We begin the treatment of the phase diagram for the case of a long junction, for $L_0 \gg \lambda_{J0}$ and $L_\pi \gg \lambda_{J\pi}$. In this case the spatial phase distribution in the ground state $\phi(x)$ is given by two fluxon tails matching at $x = 0$ (see Appendix A for details).

To investigate the phase plane in the long-junction limit, we calculate the dependence $L_\pi(L_0)$ by using the ground-state phase dependence $\varphi(L_0, L_\pi)$ obtained in Appendix C,

$$L_\pi = \frac{\varphi}{\pi - \varphi}L_0 + \Delta L_\pi, \quad (40)$$

where

$$\begin{aligned} \Delta L_\pi = & \frac{\lambda_{J0}}{\varphi - \pi} [4 \ln(z_0) \arctan(z_0) + M(z_0)] \\ & + \frac{\lambda_{J\pi}}{\pi - \varphi} [\ln(z_\pi)(2\pi - 4 \arctan(z_0)) - M(1/z_\pi)], \end{aligned} \quad (41)$$

and the function $M(z)$ (see Appendix B) is given by the integral

$$M(z) = - \int_0^z \frac{\ln(u)}{1+u^2} du. \quad (42)$$

In the local normalization a similar calculation results in

$$\ell_\pi = \frac{\varphi}{\pi - \varphi} \ell_0 \sqrt{\frac{j_{c\pi}}{j_{c0}}} + \Delta \ell_\pi, \quad (43)$$

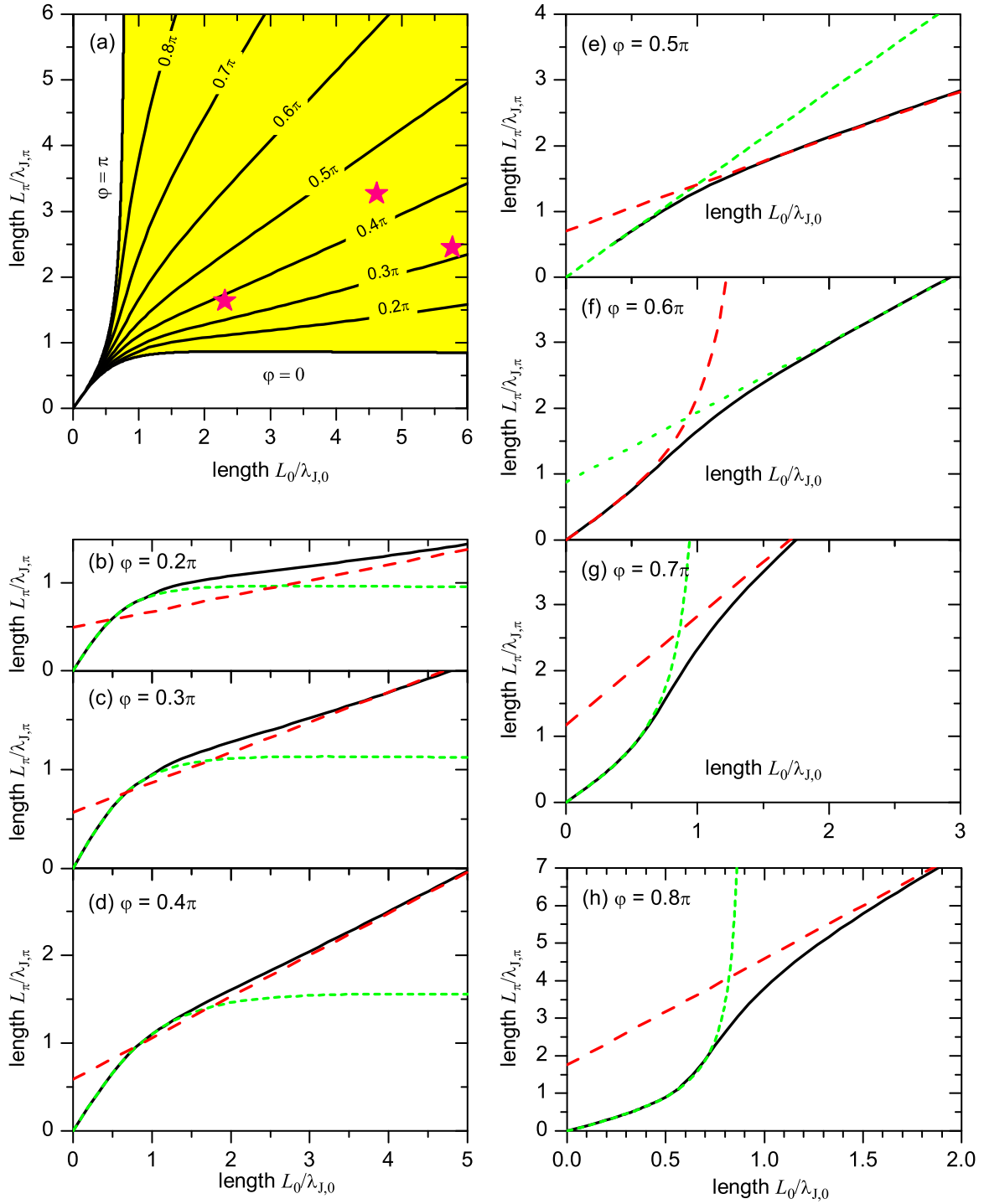


FIG. 4. (Color online) Phase diagrams calculated for the case $j_{c0} = 2j_{c\pi}$. (a) Contour lines of constant ground-state phase φ calculated numerically (solid lines). The numbers interrupting the lines indicate the values of φ . The filled region is the domain of interest where the phase smoothly changes between 0 and π . The stars show the parameters of samples d, e, and f from Table I. (b)–(h) Comparison between the numerically calculated solid lines of constant phase with those calculated analytically in the short limit (green short dashed lines) and long limit (red dashed lines).

where

$$\Delta\ell_\pi = \frac{-1}{\pi - \varphi} [4 \ln(z_0) \arctan(z_0) + M(z_0)] \sqrt{\frac{j_{c\pi}}{j_{c0}}} + \frac{-1}{\pi - \varphi} [\ln(z_\pi)(2\pi - 4 \arctan(z_0)) - M(1/z_\pi)]. \quad (44)$$

We note that for $j_{c0} = j_{c\pi}$ the values $z_0 = \sqrt{2} - 1$, $z_\pi = \sqrt{2} + 1$, so that $z_\pi = 1/z_0$, and after simple algebra, $\Delta\ell_\pi = 0$. This means that constant phase contours in the long junction limit become straight lines with a slope of $\varphi/(\pi - \varphi)$.

V. CONCLUSIONS

We have obtained the current-phase relation and studied the phase diagram (including mapping of the ground state phase) theoretically and numerically for the various possible regimes of a $0-\pi$ JJ. The limiting cases of short and long JJs are considered analytically. The intermediate region of parameters is studied numerically. The case of critical current densities $j_{c0} \neq j_{c\pi}$ relevant for experiments [12] is treated. Obtaining the CPR is crucial for a proper analysis of experiments in such junctions. Ground-state mapping is necessary for the proper selection of junction parameters in future experiments. It would also be useful to map the depth of the φ -state energy well and its asymmetry.

ACKNOWLEDGMENT

The support of Deutsche Forschungsgemeinschaft (via Project No. GO-1106/5 and SFB TRR-21) is gratefully acknowledged.

APPENDIX A: SEMIFLUXON IN A LONG $0-\pi$ JJ

Consider an infinite $0-\pi$ LJJ with $j_{c0} \neq j_{c\pi}$. The 0 part is located at $x < 0$ and the π part at $x > 0$. We assume zero magnetic field and we treat the case with no bias current. Then the phase is given by the fluxon tails,

$$\phi(x) = \begin{cases} 4 \arctan \exp\left(\frac{x-x_0}{\lambda_{J0}}\right), & x < 0, \\ 4 \arctan \exp\left(\frac{x-x_\pi}{\lambda_{J\pi}}\right) - \pi, & x > 0. \end{cases} \quad (\text{A1})$$

At $x = 0$ the phase and its derivative (proportional to the magnetic field) are continuous,

$$\arctan(z_0) = \arctan(z_\pi) - \frac{\pi}{4}, \quad (\text{A2})$$

$$\frac{1}{\lambda_{J0}} \frac{z_0}{1+z_0^2} = \frac{1}{\lambda_{J\pi}} \frac{z_\pi}{1+z_\pi^2}, \quad (\text{A3})$$

where

$$z_0 = \exp\left(-\frac{x_0}{\lambda_{J0}}\right), \quad z_\pi = \exp\left(-\frac{x_\pi}{\lambda_{J\pi}}\right). \quad (\text{A4})$$

It follows from Eq. (A2) that

$$z_0 = \frac{z_\pi - 1}{z_\pi + 1}, \quad (\text{A5})$$

$$\frac{1}{\lambda_{J0}} \frac{z_0}{1+z_0^2} = \frac{1}{\lambda_{J\pi}} \frac{z_\pi}{1+z_\pi^2}. \quad (\text{A6})$$

Solving Eqs. (A5) and (A6) we obtain

$$z_\pi = \sqrt{\frac{j_{c\pi}}{j_{c0}} + 1} + \sqrt{\frac{j_{c\pi}}{j_{c0}}} \geq 1, \quad (\text{A7})$$

$$z_0 = \sqrt{\frac{j_{c0}}{j_{c\pi}} + 1} - \sqrt{\frac{j_{c0}}{j_{c\pi}}} \leq 1. \quad (\text{A8})$$

Combining Eqs. (A7), (A8), and (A9) we find

$$x_\pi = -\lambda_{J\pi} \ln \left(\sqrt{\frac{j_{c\pi}}{j_{c0}} + 1} + \sqrt{\frac{j_{c\pi}}{j_{c0}}} \right) \leq 0, \quad (\text{A9})$$

$$x_0 = -\lambda_{J0} \ln \left(\sqrt{\frac{j_{c0}}{j_{c\pi}} + 1} - \sqrt{\frac{j_{c0}}{j_{c\pi}}} \right) \geq 0. \quad (\text{A10})$$

Now, that we have the spatial dependence of the phase we can calculate its average value as function of the facet lengths, as we do in Appendix C, and then get the phase diagram in the long junction limit.

APPENDIX B: THE FUNCTION $M(z)$

It is useful to introduce the function $M(z)$ before continuing with the averaging integral. Consider the function $M(z)$ is given by the integral

$$M(z) = - \int_0^z \frac{\ln(u)}{1+u^2} du. \quad (\text{B1})$$

Introducing a new variable $v = 1/u$ we find that

$$M(z) = M(1/z). \quad (\text{B2})$$

It follows from Eq. (B2) that $M(0) = M(+\infty) = 0$.

In the interval $0 < z < 1$ the integrand in Eq. (B1) can be written as the series

$$\frac{\ln(u)}{1+u^2} = \sum_{n=0}^{\infty} (-1)^n u^{2n} \ln(u). \quad (\text{B3})$$

Integrating the series given by Eq. (B3) we obtain

$$M_N(z) = - \sum_{n=0}^N (-1)^n \frac{z^{2n+1}}{(2n+1)^2} [(2n+1) \ln z - 1]. \quad (\text{B4})$$

If $z < 1$ then the series of Eq. (B4) is converging rapidly and $M(z) = M_\infty(z)$. If $z > 1$ then we use the relation given by Eq. (B2) and obtain the function $M(z)$ in the form $M(z) = M_\infty(1/z)$.

The sum Eq. (B3) is converging rapidly. As a result, it can be approximated by taking only a few first terms of the series. The plots of $M(z)$ and its approximation by a finite number of terms N are shown in Fig. 5. It is seen that the deviation of

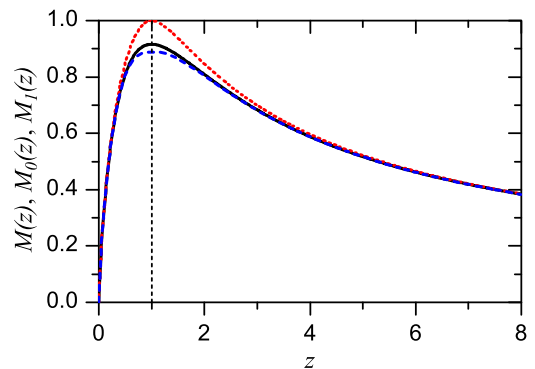


FIG. 5. (Color online) The function $M(z)$ (continuous line) calculated directly from definition Eq. (B1) and its approximations $M_0(z)$ (dotted line) and $M_1(z)$ (dashed line) calculated by using Eq. (B4).

$M_N(z)$ from $M_\infty(z)$ is less than a few percent even for $N = 0$. As a result, for most practical purposes the function $M(z)$ can be approximated as $M(z) \approx M_1(z)$.

APPENDIX C: GROUND-STATE PHASE IN THE LONG-JUNCTION LIMIT

To investigate the phase plane in the long-junction limit, we first need to find the dependence of the ground-state phase $\varphi(L_0, L_\pi)$ at $L_0 \gg \lambda_{J0}$, $L_\pi \gg \lambda_{J\pi}$. Therefore, our aim is to calculate

$$\varphi \equiv \langle \phi(x) \rangle = \frac{1}{L_0 + L_\pi} \int_{-L_0}^{+L_\pi} \phi(x) dx, \quad (\text{C1})$$

in the limit of $L_0, L_\pi \rightarrow \infty$. In this limit the phase $\phi(x)$ is given by Eq. (A1).

First, we find the value of the integral in Eq. (C1) in the 0 domain; we integrate from $-L_0$ to 0 to obtain \mathcal{I}_0 . By introducing a new integration variable

$$y = \frac{x - x_0}{\lambda_{J0}} \quad (\text{C2})$$

and, correspondingly, new integration limits

$$y_0 = \frac{-x_0}{\lambda_{J0}}, \quad y_{L_0} = \frac{-L_0 - x_0}{\lambda_{J0}}, \quad (\text{C3})$$

after integration by parts, we get

$$\mathcal{I}_0 = \lambda_{J0} \left[4y \arctan e^y \Big|_{y_{L_0}}^{y_0} - \int_{y_{L_0}}^{y_0} 4 \arctan e^y dy \right]. \quad (\text{C4})$$

Further, we introduce a new integration variable, Eq. (A4),

$$z = e^y, \quad \text{so that} \quad z_0 = e^{y_0} \quad \text{and} \quad z_{L_0} = e^{y_{L_0}}, \quad (\text{C5})$$

and Eq. (C4) turns into

$$\mathcal{I}_0 = \lambda_{J0} \left[4 \ln(z) \arctan(z) \Big|_{z_{L_0}}^{z_0} - 4 \int_{z_{L_0}}^{z_0} \frac{\ln z}{1+z^2} dz \right]. \quad (\text{C6})$$

The value of z_{L_0} is exponentially small for large L_0 . Therefore, $\ln(z_{L_0}) \arctan(z_{L_0})$ as well as the lower integration limit z_{L_0} can be substituted by 0 with exponential accuracy. Thus, we obtain

$$\mathcal{I}_0 = \lambda_{J0} [4 \ln(z_0) \arctan(z_0) + 4\mathcal{M}(z_0)], \quad (\text{C7})$$

where the function $M(z)$ is defined by Eq. (B1) and can be calculated as discussed in Appendix B. Note that according to Eq. (A8) $z_0 < 1$, one can take a series $\mathcal{M}_N(z_0)$; see Eq. (B4).

The calculation of the average phase in the π domain follows the same procedure. Now we introduce

$$y = \frac{x - x_\pi}{\lambda_{J\pi}} \quad (\text{C8})$$

and, correspondingly, new integration limits

$$y_\pi = \frac{-x_\pi}{\lambda_{J\pi}}, \quad y_{L_\pi} = \frac{L_\pi - x_\pi}{\lambda_{J\pi}}. \quad (\text{C9})$$

After integration by parts, we get

$$\mathcal{I}_\pi = -\pi L_\pi + \lambda_{J\pi} \left[4y \arctan e^y \Big|_{y_\pi}^{y_{L_\pi}} - \int_{y_\pi}^{y_{L_\pi}} 4 \arctan e^y dy \right]. \quad (\text{C10})$$

Further, we introduce a new integration variable, Eq. (A4),

$$z = e^y, \quad \text{so that} \quad z_\pi = e^{y_\pi} \quad \text{and} \quad z_{L_\pi} = e^{y_{L_\pi}}, \quad (\text{C11})$$

and Eq. (C10) turns into

$$\mathcal{I}_\pi = -\pi L_\pi + \lambda_{J\pi} \left[4 \ln(z) \arctan(z) \Big|_{z_\pi}^{z_{L_\pi}} - 4 \int_{z_\pi}^{z_{L_\pi}} \frac{\ln z}{1+z^2} dz \right]. \quad (\text{C12})$$

The value of z_{L_π} is exponentially large so that the limit of integration can be substituted by $+\infty$ and $\arctan(z_{L_\pi})$ can be substituted by 2π with exponential accuracy. Thus, we obtain

$$\mathcal{I}_\pi = -\pi L_\pi + \lambda_{J\pi} \left[2\pi \ln(z_{L_\pi}) - 4 \ln(z_\pi) \arctan(z_\pi) - 4\mathcal{M}(z_\pi) \right]. \quad (\text{C13})$$

By using the definition Eqs. (C9) and (C11), the first term in the braces can be expanded to obtain L_π explicitly. Further, according to Eq. (A7) $z_\pi > 1$, one should make use of relation Eq. (B2) and obtain

$$\mathcal{I}_\pi = +\pi L_\pi + \lambda_{J\pi} [\ln(z_\pi)(2\pi - 4 \arctan(z_\pi)) - 4\mathcal{M}(1/z_\pi)]. \quad (\text{C14})$$

Finally, combining Eqs. (C7) and (C14) and embedding them into Eq. (C1) we obtain

$$\varphi = \frac{\mathcal{I}_0 + \mathcal{I}_\pi}{L_0 + L_\pi} = \frac{\lambda_{J0} [4 \ln(z_0) \arctan(z_0) + 4\mathcal{M}(z_0)] + \pi L_\pi + \lambda_{J\pi} \{ \ln(z_\pi) [2\pi - 4 \arctan(z_\pi)] - 4\mathcal{M}(1/z_\pi) \}}{L_0 + L_\pi}. \quad (\text{C15})$$

Note that the values of z_0, z_π in Eq. (C15) are just constants defined by j_{c0} and $j_{c\pi}$ and given by Eqs. (A7) and (A8).

- [1] L. N. Bulaevskii, V. V. Kuzii, and A. A. Sobyenin, *JETP Lett.* **25**, 290 (1977).
 [2] V. B. Geshkenbein, A. I. Larkin, and A. Barone, *Phys. Rev. B* **36**, 235 (1987).
 [3] V. V. Ryazanov, V. A. Oboznov, A. Y. Rusanov, A. V. Veretennikov, A. A. Golubov, and J. Aarts, *Phys. Rev. Lett.* **86**, 2427 (2001).
 [4] T. Kontos, M. Aprili, J. Lesueur, F. Genêt, B. Stephanidis, and R. Boursier, *Phys. Rev. Lett.* **89**, 137007 (2002).

- [5] M. Weides, M. Kemmler, E. Goldobin, D. Koelle, R. Kleiner, H. Kohlstedt, and A. Buzdin, *Appl. Phys. Lett.* **89**, 122511 (2006).
 [6] J. A. van Dam, Y. V. Nazarov, E. P. A. M. Bakkers, S. De Franceschi, and L. P. Kouwenhoven, *Nature (London)* **442**, 667 (2006).
 [7] H. Jorgensen, T. Novotny, K. Grove-Rasmussen, K. Flensberg, and P. Lindelof, *Nano Lett.* **7**, 2441 (2007).
 [8] A. Buzdin and A. E. Koshelev, *Phys. Rev. B* **67**, 220504(R) (2003).

- [9] A. Gumann and N. Schopohl, *Phys. Rev. B* **79**, 144505 (2009).
- [10] N. G. Pugach, E. Goldobin, R. Kleiner, and D. Koelle, *Phys. Rev. B* **81**, 104513 (2010).
- [11] E. Goldobin, D. Koelle, R. Kleiner, and R. G. Mints, *Phys. Rev. Lett.* **107**, 227001 (2011).
- [12] H. Sickinger, A. Lipman, M. Weides, R. G. Mints, H. Kohlstedt, D. Koelle, R. Kleiner, and E. Goldobin, *Phys. Rev. Lett.* **109**, 107002 (2012).
- [13] E. Goldobin, H. Sickinger, M. Weides, N. Ruppelt, H. Kohlstedt, R. Kleiner, and D. Koelle, *Appl. Phys. Lett.* **102**, 242602 (2013).
- [14] R. G. Mints, I. Papiashvili, J. R. Kirtley, H. Hilgenkamp, G. Hammerl, and J. Mannhart, *Phys. Rev. Lett.* **89**, 067004 (2002).
- [15] R. G. Mints, *Phys. Rev. B* **57**, R3221 (1998).
- [16] R. G. Mints and I. Papiashvili, *Phys. Rev. B* **64**, 134501 (2001).
- [17] E. Goldobin, D. Koelle, R. Kleiner, and A. Buzdin, *Phys. Rev. B* **76**, 224523 (2007).
- [18] E. Goldobin, R. Kleiner, D. Koelle, and R. G. Mints, *Phys. Rev. Lett.* **111**, 057004 (2013).
- [19] H.-J. H. Smilde, Ariando, D. H. A. Blank, G. J. Gerritsma, H. Hilgenkamp, and H. Rogalla, *Phys. Rev. Lett.* **88**, 057004 (2002).
- [20] Ariando, D. Darminto, H.-J. H. Smilde, V. Leca, D. H. A. Blank, H. Rogalla, and H. Hilgenkamp, *Phys. Rev. Lett.* **94**, 167001 (2005).
- [21] S. Scharinger, M. Turad, A. Stöhr, V. Leca, E. Goldobin, R. G. Mints, D. Koelle, and R. Kleiner, *Phys. Rev. B* **86**, 144531 (2012).
- [22] M. Weides, M. Kemmler, H. Kohlstedt, R. Waser, D. Koelle, R. Kleiner, and E. Goldobin, *Phys. Rev. Lett.* **97**, 247001 (2006).
- [23] M. Weides, U. Peralagu, H. Kohlstedt, J. Pfeiffer, M. Kemmler, C. Gürlich, E. Goldobin, D. Koelle, and R. Kleiner, *Supercond. Sci. Technol.* **23**, 095007 (2010).
- [24] M. Kemmler *et al.*, *Phys. Rev. B* **81**, 054522 (2010).
- [25] L. N. Bulaevskii, V. V. Kuzii, and A. A. Sobyenin, *Solid State Commun.* **25**, 1053 (1978).
- [26] E. Goldobin, R. Kleiner, and D. Koelle, *Phys. Rev. B* **87**, 224501 (2013).